Research article

SURFACE and INTERFACE ANALYSIS

Received: 15 February 2012 Accepted: 24 May 2012 Published online in Wiley Online Library: 22 June 2012

(wileyonlinelibrary.com) DOI 10.1002/sia.5075

Photo-induced surface transformations of silica nanocomposites

Justin M. Gorham,[a]* Tinh Nguyen,[b] Coralie Bernard,[b] Debbie Stanley[b] and R. David Holbrook[a]

The photo-induced, physicochemical surface transformations to silica nanoparticle (SiNP) - epoxy composites have been investigated. The silica nanocomposites (SiNCs) were prepared using a two-part epoxy system with a 10% mass fraction of SiNPs and exposed to varying doses of high intensity, ultraviolet (UV) radiation at wavelengths representative of the solar spectrum at sea level (290 nm to 400 nm) under constant temperature and humidity. Visibly apparent physical modifications to the SiNC surface were imaged with scanning electron microscopy. Surface pitting and cracking became more apparent with increased UV exposure. Elemental and surface chemical characterization of the SiNCs was accomplished through X-ray energy dispersive spectroscopy and X-ray photoelectron spectroscopy, while attenuated total reflectance Fourier transform infrared spectroscopy revealed changes to the epoxy's structure. During short UV exposures, there was an increase in the epoxy's overall oxidation, which was accompanied by a slight rise in the silicon and oxygen components and a decrease in overall carbon content. The initial carbon components (e.g. aliphatic, aromatic and alcohol/ether functionalities) decreased and more highly oxidized functional groups increased until sufficiently long exposures at which point the surface composition became nearly constant. At long exposure times, the SiNC's silicon concentration increased to form a surface layer composed of approximately 75% silica (by mass). Published 2012. This article is a U.S. Government work and is in the public domain in the USA.

Supporting information may be found in the online version of this article.

Keywords: silica nanoparticles; nanocomposites; environmental; surface analysis; UV degradation

Introduction

Development of nanomaterials for novel applications has been the focus of many research efforts over the past two decades due to the properties materials possess upon approaching the nanoscale regime (less than 100 nm). One particular application is to incorporate nanomaterials into polymeric materials to form polymer nanocomposites (NCs). NCs are films or structures made up of two components: a major component (e.g. metal, ceramic, polymer) that forms a matrix in which a minor component composed of nanofillers (e.g. carbon nanotubes, iron oxide, silica nanoparticles) may be dispersed.[1] The incorporation of nanofillers into a polymeric matrix typically achieves highly desirable improvements in their material and physicochemical properties.

Silica nanoparticles (SiNPs), for example, have been incorporated into polymeric matrices and foams to enhance their flame-retardant properties.[1,2] In the automotive, plastics, paper, and flooring industries, SiNPs and other inorganic materials have been incorporated into polymeric coatings to enhance their resistance to chemical and mechanical damages.[1,3–5] These silica NC (SiNC) coatings can increase hardness, wear resistance and fracture toughness with relatively low percentages of SiNPs incorporated into polymers.[6–8] Polyacrylate-based and other inorganic materials SiNCs exhibited improved electrical resistivity compared to traditional counterparts, resulting in a more energy efficient, organic light-emitting devices.[1] While SiNCs have many beneficial properties for surface coatings or devices, they are hardly perfect without optimization of their chemical composition. Specifically, some material and mechanical properties can decline when excessive amounts of SiNPs are added.[1] For example, poly(methyl methacrylate)-based SiNCs decreased fracture toughness $>25\%$ as a result of increasing the SiNP mass from 10% to 20% of the total composite mass fraction. [6]

Variations in the composition of SiNCs are not solely a result of manufacturing and production, but may occur due to transformations over the course of their life cycles. Specifically, many polymers have a propensity to degrade depending upon environmental conditions.[9] For example, phosphorous-implanted polyethylene oxidizes upon exposure to atmospheric and atomic oxygen radicals, ultimately enhancing its resistance to further oxidative degradation.[10] Another well-known route of transformations of polymeric materials includes mechanisms involving the ultraviolet (UV) component of sunlight.[9,11] The exposure of many polymers to UV radiation between 290 and 400 nm can chemically and physically modify the polymers via photo-oxidation leading to mass loss and changes in materials properties such as increased brittleness. [12]

The photodegradation of epoxy, an important class of polymeric materials, such as those that include diglycidal ether of bisphenol A (DGEBA) have also been investigated.[13–16] It was found that the epoxy compounds undergo oxidative photodegradation via gas phased species (e.g. O_2, H_2O), where one

* Correspondence to: Justin M. Gorham, Material Measurement Laboratory, National Institute of Standards and Technology. E-mail: justin.gorham@nist.gov

a Material Measurement Laboratory, National Institute of Standards and Technology

b Engineering Laboratory, National Institute of Standards and Technology

Published 2012. This article is a U.S. Government work and is in the public domain in the USA.

mechanism postulated was chain scission.[13,16] Similar epoxies have been employed in the preparations of SiNCs to determine the potential for NP release due to exposure by simulated solar radiation.[17,18] After UV exposure, the SiNCs increased in mass fraction of SiNPs, exhibited photodegradation of the polymeric matrix, demonstrated a measurable mass loss and provided clear evidence for SiNP release.[18] The loss of SiNPs from a NC surface raises nanomaterial-related environmental, health and safety (nanoEHS) concerns about their fate once put into service. While there have been investigations on the degradation of SiNCs by reactive species such as UV radiation, the physical and chemical transformations at the material's surface ($<$ 10 nm), the most likely location of release of NPs into the environment, have not been extensively explored. Further research focused on elucidating photo-induced, surface chemical processes would provide (i) guidance on the modifications needed to prevent photodegradation and (ii) a timeline for material replacement prior to NP release, thereby providing a first step towards alleviating nanoEHS concerns.

The focus of this study was to investigate the surface transformations of SiNCs caused by exposure to high intensity light from the Simulated Photodegradation via High Energy Radiant Exposure (SPHERE) representative of the UV component of solar radiation. SiNCs were prepared and photodegraded under controlled conditions and analyzed using a suite of surface analytical techniques. Scanning electron microscopy (SEM) and atomic force microscopy (AFM) were used to observe surface morphological transformations, while X-ray photoelectron spectroscopy (XPS) was employed to track surface chemical changes. Additional data from energy dispersive spectroscopy (EDS) and attenuated total reflectance Fourier transform infrared spectroscopy (ATR-FTIR) are presented to provide supplementary, semi-surface sensitive data on elemental and chemical modifications, respectively.

Experimental[1]

Materials and nanocomposite preparation

The details of the preparation of SiNP/ epoxy composites can be found in references.[17,18] Briefly, 7-nm nanosilica (Aerosil R812, Evonik) modified with hexamethyl disilazane (HMDS) was employed[1]. The epoxy was formed from DGEBA resin (Epon 828, Resolution Performance Products) and a tri-poly(ether amine) curing agent (Jeffamine T403, Huntsman Corporation). SiNPs were originally suspended in toluene and mixed with a tip sonicator for 30 min when the appropriate masses of the epoxy resin and curing agent were added to the SiNP suspension under constant magnetic stirring. After combining the DGEBA and tri-poly(ether amine), the mixture was sonicated and stirred for an additional hour. The amount of epoxy components added was sufficient to generate a 10% mass fraction of SiNCs. After the mixing step, the epoxy/nanosilica mixture was degassed for 1 h at room temperature and then drawn down on a polyethylene terephthalate sheet (Mylar) (a good release substrate for epoxy-base materials). SiNCs were cured at ambient conditions (24 °C and 50% relative humidity) for three days, followed by post-curing for 4 h at 110 °C in an air circulating oven. After curing, free standing SiNC films having a thickness of between 150 μm and 200 μm were removed from the substrate. The glass transition temperature of this amine-cured epoxy was 102 °C $\pm$ 2 °C (average and one standard deviation), as measured by dynamic mechanical analysis technique. It is noted that no UV stabilizer was added to the epoxy SiNCs used in this study.

UV-exposure conditions

All samples were exposed to the UV component of solar radiation on the NIST SPHERE.[19] The SPHERE is based on integrating sphere technology and generates a collimated, uniform flux of photons representative of the UV component of the solar spectrum at 22 times the irradiance of the sun. Cutoff filters are in place to remove the non-solar component of the UV light generated to ensure that the wavelengths exposed to samples were in the 290 nm to 400 nm range. During UV exposure, the SiNCs were exposed to varying doses of UV radiation, for up to 72 days, in ports around the NIST SPHERE. These ports were controlled for both temperature and relative humidity which were set to 50 °C and 75%, respectively. Each port was capable of containing up to 17 samples so by simply operating multiple ports at identical conditions, the samples could be exposed concurrently as to avoid any day-to-day variation in the UV source. Samples were removed at specific time intervals for characterization.

Characterization techniques

Scanning electron microscopy

Images of select samples were acquired using a Quanta 200 Field Emission Gun (FEG) environmental SEM (FEI, Hillsboro, OR). Prior to imaging, all samples were sputter coated with a thin layer ($\approx$5 nm) of gold to mitigate sample charging and damage from the electron beam. Images were collected at an accelerating voltage of 10 kV. In addition to imaging, X-ray EDS was performed using a silicon drift detector (30 mm^2) (Bruker, Madison, WI) for bulk (up to at least 2500-nm sampling depth) information on the relative changes in the SiNC samples' elemental distribution with increasing SPHERE exposure. All spectra acquired were analyzed using DTSA-II software for element identification and qualitative transformations,[20] and the spectra were normalized to the total measured X-ray intensity through 5004 eV.

Atomic force microscopy

AFM measurements were carried out at ambient conditions (24 °C, 45% relative humidity) using a Nanoscope Dimension 3100 system (Bruker AXS, Madison, WI). Samples were prepared by mounting the exposed material to a glass slide using double-sided tape to reduce noise from sample movement. Tips were commercial Si micro cantilever probes obtained from Olympus (Model AC160TS, Center Valley, PA) with a spring constant of 42 N/m, 9 nm tip radius and a resonance frequency of approximately 300 kHz. Both topographic and phase images were obtained simultaneously using a free-oscillation amplitude of 62 nm $\pm$ 2 nm (average and 1 standard deviation). Root mean square (RMS) roughness values were obtained from 20 μm $\times$ 20 μm scans. Measurements of surface defects represented an average and standard deviation of over ten measurements.

[1]Certain trade names and company products are mentioned in the text or identified in illustrations in order to specify adequately the experimental procedure and equipment used. In no case does such identification imply recommendation or endorsement by National Institute of Standards and Technology, nor does it imply that the products are necessarily the best available for the purpose.

 Published 2012. This article is a U.S. Government work and is in the public domain in the USA.

X-ray photoelectron spectroscopy

To prepare samples for XPS, exposed SiNC were mounted to a sample bar with double-sided carbon tape. These samples were pumped down in an introductory chamber before being introduced into the main chamber where the bar was placed on a fork with capabilities for x, y, z and rotational adjustments. The base pressure in the main analysis chamber was 2.66×10^{-7} Pa, and the samples were prevented from charging during the experiment through use of low energy electrons (1.8 A and 2.5 V).

Data acquisition was conducted using a Kratos Axis Ultra DLD spectrometer (Chestnut Ridge, NY) that is equipped with a monochromatic Al K α source (1486.6 eV) and a hemispherical analyzer collecting photoelectrons zero degrees from the surface normal. Each sample was measured twice; initially, full spectra were acquired using a pass energy of 160 eV (1.0 eV/step) to determine the identity of all elements present, and finally, multiplexes of specific elemental regions were taken at a pass energy of 40 eV (0.1 eV/step). Values and spectra presented in this study are from multiplex conditions unless otherwise stated.

Data analysis took place using Casa XPS. Specifically, the C (1s), Si (2p), N (1s) and O (1s) regions were fit with a Shirley background, referenced to the N (1s) peak at 400 eV[21], and area adjusted using relative sensitivity factors of 0.278, 0.328, 0.477 and 0.780, respectively. Peak fitting of the C (1s) region was performed using three, 100% Gaussian peaks representing different functionalities. An additional π- π^* transition was identified, but not quantified, between 291 and 292 eV. All measurements of percent concentrations and peak positions are based on an average of the measurements. The reported error values reflect ± 1 standard deviation when at least three measurements ($t = (0, 8, 65, 72)$ d) were taken and the range when only two measurements ($t = (14, 24, 35, 48)$ d) were taken, with the exception of the data taken at 4 d of exposure which was one measurement alone, unless otherwise stated.

Attenuated total reflectance-Fourier transform infrared spectroscopy

ATR-FTIR were recorded at a resolution of 4 cm^{-1} using filtered, dry air as a purge gas, a Durascope ATR accessory (SensIR Technologies) and a FTIR spectrometer (Nexus 670, Thermo Nicolet, Madison, WI) equipped with a liquid nitrogen-cooled mercury cadmium telluride detector. A ZnSe prism and an incident angle of 45º were used for all ATR-FTIR measurement. All spectra presented are the average of 128 scans which were normalized to 1 at the stable peak of 1362 cm^{-1}. The peak height was used to represent the infrared intensity, and their respective functional groups. All plotted ATR-FTIR intensity results were the average and standard deviation of four specimens. For the intensities measured at (2965, 1508 and 1083) cm^{-1}, the intensity of the samples was normalized in addition to the one based on the unexposed sample to obtain relative transformations.

Results

Morphological and elemental transformations

Over the course of this study, after the SiNCs were irradiated with simulated solar radiation and removed from the sample holder, they were stored in the dark until analyzed. Visual observation revealed that the UV-exposed surface began to show signs of degradation after eight days. As UV exposure increased, signs of degradation became more evident as characterized by an initial discoloration of the SiNC surface. At the longest UV exposures, the SiNCs appeared as a deep yellow color, and the sample became brittle. The unexposed side of the SiNCs, however, did not exhibit any visual signs of degradation.

To gain a better understanding of the UV-induced discoloration of the SiNCs, select samples with varying durations of UV exposure were imaged using SEM to investigate changes in morphological characteristics. Images of the sample prior to UV exposure (Fig. 1A, Left, 0 Days) revealed a relatively smooth, clean surface devoid of any major features. Perhaps, the only surface features observed in the unexposed SiNCs were the presence of a few isolated particles and/or aggregates in the range of tens to hundreds of nanometers, most likely from aggregated SiNPs. However, while the majority of the sample surface appeared to be fairly uniform, there was some evidence for aggregate 'networks' present when viewed with high contrast (Fig. 1A, Left).

As the SiNCs were exposed to UV radiation, the surface developed a much rougher and irregular morphology. Indeed, at 14 d of exposure (Fig. 1A, Center), a network of mounds and pits formed on the surface that were irregular in shape, structure and size and appeared to be a collection of SiNP aggregates at the surface. Some images revealed signs of cracking at this point (SI Fig. S1). Transformations to the surface continued as UV exposure increased to 72 d (Fig. 1A, Right) with the morphology changed to include irregularly shaped plate-like structures. These plate-like structures had the appearance of smooth surfaces that ranged in size from less than 1 μm to large features hundreds of μm in size (SI Fig. S2). These observations clearly demonstrate that the photodegradation of the SiNCs resulted in morphological transformations.

To determine the effect of UV radiation on the SiNC composition, the imaged samples were analyzed with EDS to probe for elemental transformations (Fig. 1B). For all samples analyzed, the only elements identified were C, O and Si with a small, additional contribution from the gold coating. As the samples transformed morphologically, the elemental distribution also exhibited photo-induced modifications. Specifically, the carbon content of the SiNCs decreased with exposure while the Si and O content increased. Qualitatively, this suggests that the SiNCs underwent photodegradation via removal of at least some of the epoxy-based carbon, thereby uncovering the SiNPs underneath.

AFM images and measurements in Fig. 2 confirmed the increase in surface roughness due to UV exposure. Indeed, for the displayed SiNCs, the RMS roughness was measured to be (13.09, 30.47 and 129.3) nm for (0, 4 and 48) d for UV exposure, respectively. Interestingly, prior to exposure, the phase image showed islands of material that exhibits harder characteristics (Fig. 2 A, right inset). At short UV exposures (Fig. 2 B), topographic images revealed the presence of pits, which can be observed more clearly from the insets, measured to be (49.5 ± 10.2) nm and demonstrated a clear change in phase, in agreement with SEM analysis. Long UV exposures were also consistent, resulting in a highly roughened surface (Fig. 2 C). In combination, Figs. 1 and 2 confirm that photodegradation resulted in morphological and elemental changes due to carbon removal and increased SiNP mass fractions at least at the SiNC surface.

Surface chemical transformations

XPS analysis was chosen to examine the surface chemical transformations to the SiNCs. In Fig. 3, representative high-resolution XP spectra for the O (1s), N (1s), C (1s) and Si (2p) regions are

Published 2012. This article is a U.S. Government work and is in the public domain in the USA.

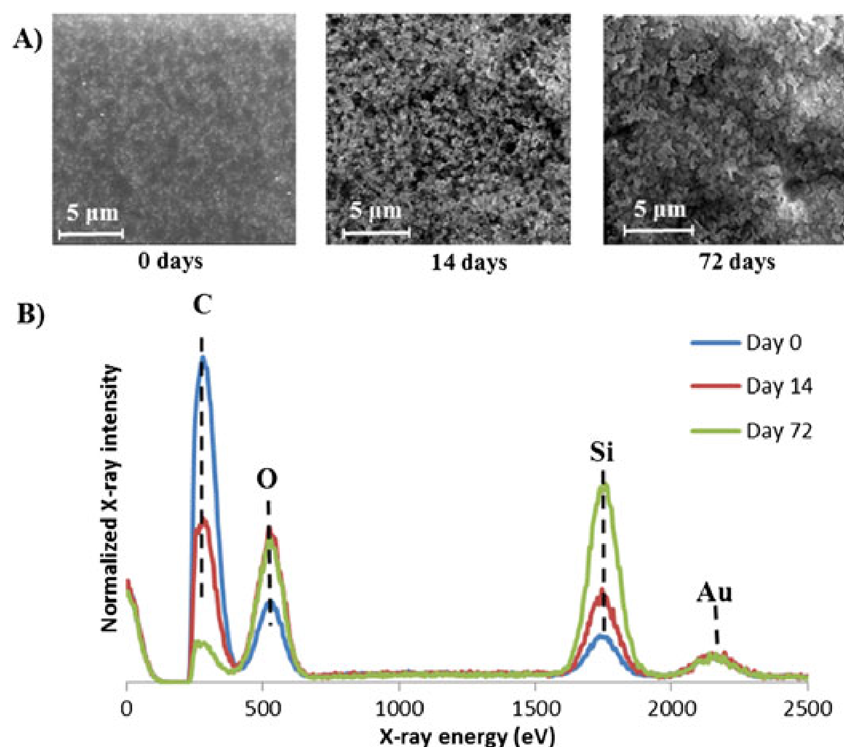

Figure 1. A) Representative SEM images of 10% (by mass) SiNP-epoxy composites taken at 0 days, 14 days and 72 days of exposure to UV radiation. B) EDS spectra of the same samples with the X-ray energy positions indicated for the C K-L3, O K-L3, Si K-L3 and Au M5-N7 lines. All spectra were normalized to the total X-ray intensity measured through 5004 eV.

displayed. Initially, the XPS peak maxima for each of the elements was located at a binding energy of (532. 8 $\pm$ 0.1) eV, (284.8 $\pm$ 0.1) eV and (102.2 $\pm$ 0.1) eV for the O (1s), C (1s) and Si (2p) spectra, respectively.[21] Prior to UV exposure, the SiNCs were predominantly composed of carbon, oxygen and nitrogen in percent concentrations of (79.07 $\pm$ 1.83) %, (16.91 $\pm$ 1.35) % and (2.33 $\pm$ 0.17) %, respectively, with a small contribution from the Si (2p) region of (1.49 $\pm$ 0.51) %. While values calculated for 10% mass fraction of SiNPs (using the representative models from the literature) were close to the aforementioned measured values based on their molar concentrations,[17,18] the Si (2p) and O (1s) percentages were lower, and the C (1s) and N (1s) values were higher than anticipated. This discrepancy may be caused by the presence of an epoxy-rich overlayer at the surface or HMDS surface modifications to the SiNPs.

Within the C (1s) region, three 100% Gaussian peaks (no Lorentzian tailoring) were assigned and constrained based on the non-UV exposed spectra (Fig. 3, third column) and comparable literature values of binding energy position for a given functional group. The aliphatic (CH_2 / C–C) component of the C (1s) region was located at (284.7 $\pm$ 0.3) eV,[22,23] and composed (49.01 $\pm$ 1.93) % of the unexposed samples. While the literature reported slightly different binding energies for carbon bound to nitrogen as opposed to carbon bound to oxygen for their peak maxima (e.g. esters *versus* amides; ethers / alcohols *versus* primary / secondary / tertiary amines), in this study, certain C functionalities were combined into one peak based on the total number of O and/or N atom bonds with a given carbon center due to instrumental limitations in distinguishing between multiple components so close in binding energies. Therefore, the remainder of the fitted spectra was assigned to oxidized carbon species, specifically C–O / C–N at(286.3 $\pm$ 0.3) eV and CO(O) / CN(O) at (288.2 $\pm$ 0.3) eV [23–25] components, which were measured to be (26.76 $\pm$ 1.49) % and (2.92 $\pm$ 0.21) % of the initial SiNCs, respectively. In addition, the π- π^* transition was identified at approximately 291 eV, which is representative of the aromaticity associated with the DGEBA component of the epoxy. An enlarged version of the C (1s) region from 290 eV to 294 eV is available in the supporting information (SI Fig. S3).

With increased UV exposure, changes in the SiNCs elemental composition (Fig. 1B) were also apparent in the XP spectra, as demonstrated in Fig. 3. Consistent with the EDS data, the O (1s) and Si (2p) XP intensities increased while the C (1s) spectra decreased with increasing UV exposure until approximately 35 days, at which point, they remained at a steady surface concentration. The N (1s) spectra exhibited a small rise until about 14 d and then slowly decreased towards its initial surface concentration. While the spectral profiles of the O (1s) and N (1s) regions did not change in shape, the Si (2p) and C (1s) regions did change with exposure. The Si (2p) peak shifted to a higher binding energy by approximately 1.1 eV to (103.3 $\pm$ 0.1) eV with a clear transition occurring at 8 d. After 14 d, the original Si (2p) peak was no longer observed. This initial Si (2p) peak could have derived from the silanizing reagent (HMDS), which functionalized the SiNC surface and has a comparable binding energy,[26–28] or another surface contaminant. However, the new peak position at 103.3 eV after exposure is consistent with the local chemical environment of the SiO_2. [29,30]

These increases in the Si (2p) region are most likely due to the UV-induced degradation and removal of the epoxy component at the SiNC surface, which were observed through transformations of the fitted C (1s) spectral profiles (Fig. 3, third column). With increasing UV exposure, the CH_2 / C–C and CO / CN components of the C (1s) region decreased while the highly oxidized carbon component (CO(O) / CN(O)) increased in surface concentration. Additionally, the π- π^* transition (Fig. S3) remained until

Published 2012. This article is a U.S. Government work and is in the public domain in the USA.

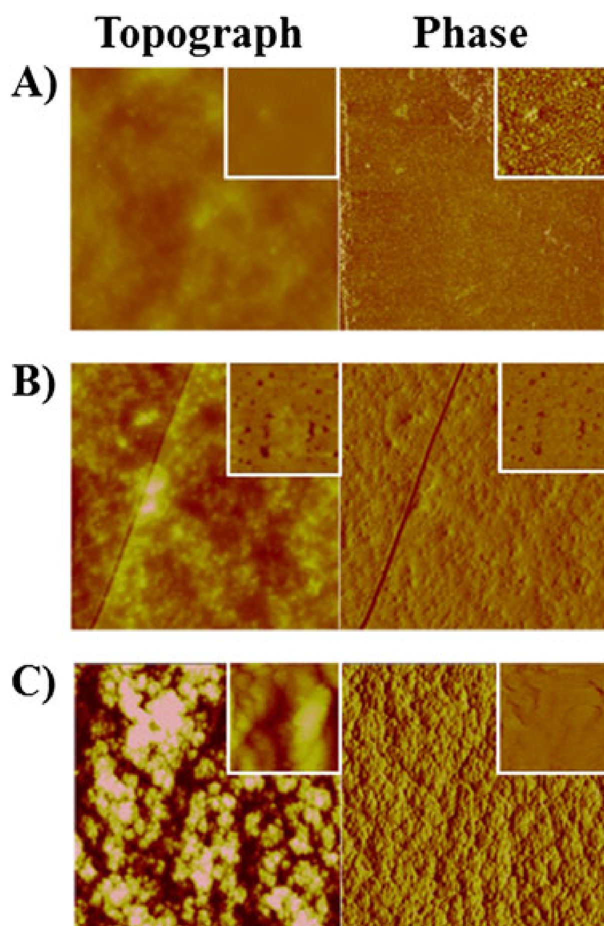

Figure 2. AFM images of SiNCs UV exposed for A) 0 d, B) 4 d and C) 48 d. For all rows, the left image is topographic (z = 400 nm) and the right image is phase with imaged areas of 20 μm × 20 μm. The insets are zoomed in images with an area of 1 μm × 1 μm (z = 200 nm).

approximately 14 d of exposure at which point it was no longer detectable, suggesting that the SiNCs aromaticity had either been removed or transformed as a result of the UV radiation.

The XPS measured transformations in the SiNCs surface chemistry are plotted as elemental and component percentages *versus* UV exposure in Figs. 4 and 5, respectively. At 4 d of exposure, no statistically significant deviations in the elemental concentrations were observed for any of the elements detected in the SiNCs (Fig. 4). From 8 d to 35 d, however, there were significant changes in the percent surface concentrations. Specifically, the O (1s) and Si (2p) regions increased during this time frame to a final composition concentration of (47.81 ± 2.26) % and (20.85 ± 1.97) %, respectively, while the decrease in the C (1s) region stabilized at a final value of (28.99 ± 3.79) % (All final percentages are indicated by the dotted lines in Figs. 4 and 5; these final values and error bars are representative of an average of all data from exposures of 35 d and greater ± 1 standard deviation). Additionally, the N (1s) region also changed with exposure, increasing from (2.33 ± 0.17) % to (3.45 ± 0.20) % between 0 d and 14 d of exposure, respectively, followed by a corresponding decrease to a final value of (2.14 ± 0.27) %.

The three main components of the C (1s) region were plotted *versus* UV exposure time (Fig. 5). The initial distribution of carbon in the SiNCs consisted of the CH_2 / CC and the CO / CN components making up (49.01 ± 1.93) % and (26.76 ± 1.49) % of the surface composition, respectively, while the CO(O) / CN(O) component composed (2.92 ± 0.21) % of the surface. Exposure to UV radiation initiated modifications in the epoxy's distribution of functionalities. Specifically, a decrease in percent surface concentration of the CO / CN component and minor increases in the C-C / CH_2 and CO(O) / CN(O) components were measured after 4 d of UV exposure (Fig. 5). Interestingly, there was no clear induction period for the changes to the components as was observed in the C (1s) elemental plots through the first four days (Fig. 4). After 4 d, both the C–C / CH_2 and C–O / C–N components decreased simultaneously following an exponential decay

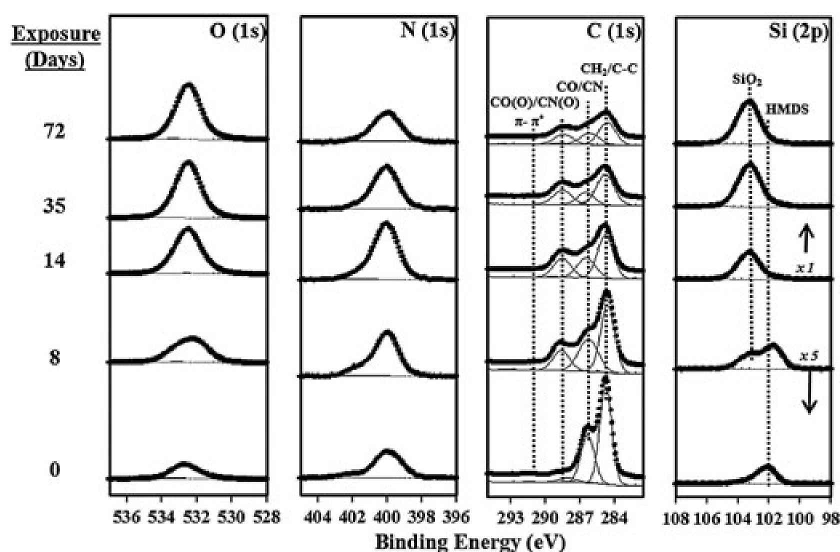

Figure 3. High-resolution XP spectra of the UV-exposed 10% (by mass) SiNP-epoxy composites. Representative samples are displayed from different exposures to illustrate changes to the elemental and chemical composition over time. The dashed, vertical lines in the C (1s) and Si (2p) regions are meant as a guide to the location of different components in those regions. The Si (2p) region counts are multiplied by five for 0 d and 8 d. The C (1s) spectra and composite fits are manually offset from the baseline for ease of viewing.

Published 2012. This article is a U.S. Government work and is in the public domain in the USA.

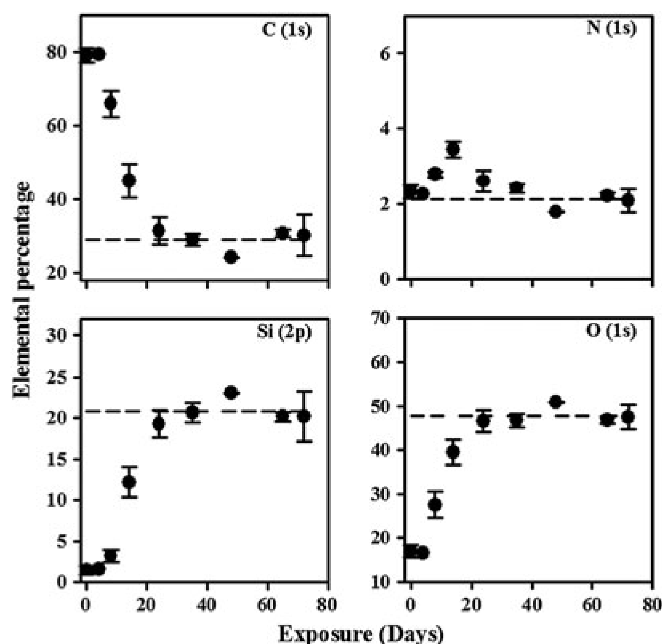

Figure 4. Plots of percent surface concentration of the N (1s), O (1s), C (1s) and the Si (2p) regions of the epoxy SiNP composite with UV exposure time. The horizontal dashed lines are meant to indicate the final, approximated percent composition of each element at long exposure, an average from day 35 and on. Values for $t = (0, 8, 65, 72)$ d are the average of at least three samples +/− 1 standard deviation. Values for $t = (14, 24, 35, 48)$ d are the average of two points, and the error represents the range. Four days was a single point.

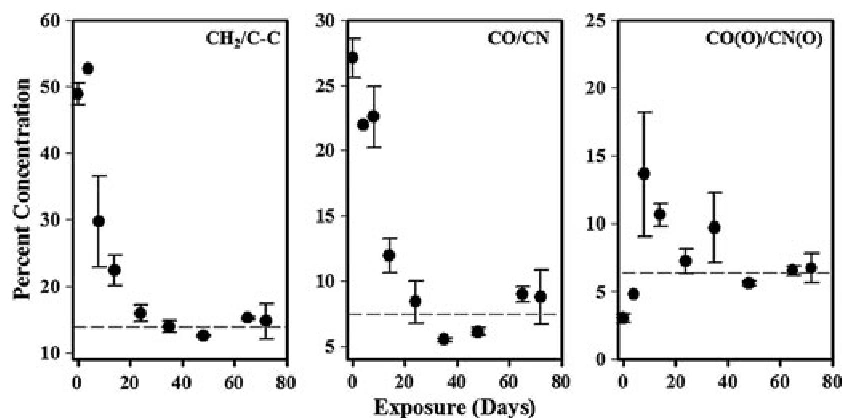

Figure 5. Plots of the surface concentrations of the components of the C (1s) region *versus* exposure time to UV radiation. The dashed lines indicate steady-state percentages. Values for $t = (0, 8, 65, 72)$ d are the average of at least three samples +/− 1 standard deviation. Values for $t = (14, 24, 35, 48)$ d are the average of two points and the error represents the range. Four days was a single point.

process, or pseudo first-order kinetics, until approximately 35 d of UV exposure to an average percent surface concentration of (13.98 ± 1.74) % and (7.17 ± 1.74) %, respectively. Conversely, the CO(O) / CN(O) component grew with UV exposure to a percent surface concentration of (14.84 ± 5.71) % at 8 d and then decreased to (6.34 ± 0.72) % after approximately 50 d.

Further insight into the mechanism of photodegradation of the SiNCs can be obtained by plotting the two primary components of the C (1s) spectra (Figs. 2 and 4) as a ratio (CO / CN: CH_2 / CC) *versus* UV exposure (Fig. 6). Consistent with the epoxy's molecular structure,[17,18] the carbon in the SiNC should contribute to the CO / CN or the CH_2 / C–C with a theoretical relative ratio of approximately 0.60, respectively, compared to the initial measured ratio of 0.55 ± 0.04. The difference may be due to surface carbon contamination or a result of the SiNP's surface modification with HMDS. For the duration of the 72 d of UV exposure, the majority of the ratios remained scattered between 0.4 and 0.6 at an average ratio of 0.56 ± 0.16 (average value and standard deviation of all points) with no discernible trend suggesting that sections of the initial epoxy structure were being removed or modified simultaneously, thereby remaining roughly constant throughout the photodegradation.

Vibrational data

To obtain further information about the chemical transformations of the SiNC during UV exposure, samples were further probed using ATR-FTIR spectroscopy. Figure 7A shows the ATR-FTIR data for UV-exposed SiNCs (0 d to 21 d, split into two plots for ease of viewing). Prior to UV exposure (day 0), peaks

Published 2012. This article is a U.S. Government work and is in the public domain in the USA.

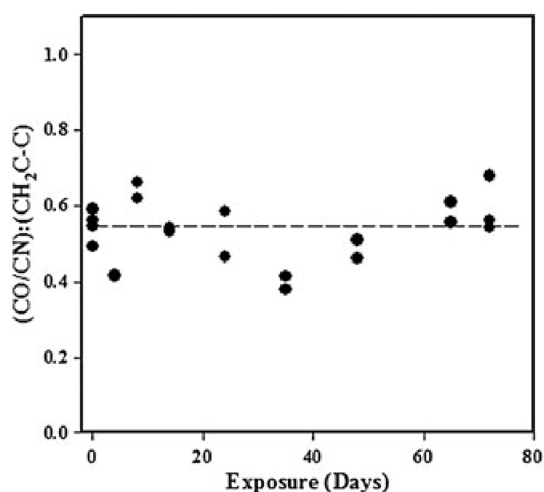

Figure 6. The ratio of the CO/CN component to the hydrocarbon components of the epoxy in the composite *versus* UV exposure for all samples analyzed. The samples have an average ratio over UV exposure at a value of 0.56 ± 0.15 which represents the average of all 19 points over 72 days +/− 1 standard deviation.

representing the different vibrational characteristics of the SiNC were found and identified. For the epoxy, ATR-FTIR intensities at approximately 826 cm^{-1}, 1244 cm^{-1} and 1508 cm^{-1} (Fig. 7A, Left) were identified as dominant bending and stretching modes observed from the aromatic component of DGEBA for C–H, C–O–C and C–C bonds, respectively (underlined carbon atoms are part of the phenyl rings).[31] Additional bands found between 1000 and 1200 cm^{-1} are typical of non-aromatic C–O stretches such as ether and alcohol groups from the epoxy structure, as well as Si–O–Si/Si–O–C, bonds representative of the SiNPs. For the purposes of this study, however, the maximum at 1083 cm^{-1} was used to monitor both functionalities.[31–33] Evidence for the tertiary amine structure can be found prior to UV exposure at 1180 cm^{-1}. Figure 7A (right) reflects the balance of the functionality observed within the SiNC. The IR spectral region between 2700 and 3000 cm^{-1} is typically representative of the non-aromatic C–H stretching modes. The broad IR band from (3100 to 3700) cm^{-1} is typically associated with various O–H stretching frequencies and N–H stretching frequencies. [31]

Upon UV exposure, the epoxy from the SiNC underwent an initial photodegradation characterized by a significant loss in the aliphatic, aromatic and the initial C–O bond characteristics. The losses in the epoxy's structure are represented in plots of the C–C, C–H and C–O stretching frequencies at 1508 cm^{-1}, 2965 cm^{-1} and 1083 cm^{-1}, respectively, *versus* UV exposure (Fig. 7B). The stretching frequencies at 2965 cm^{-1} and 1508 cm^{-1} both rapidly decreased in intensity over the first week of UV exposure, followed by a slower loss over the subsequent two weeks. The trends depicted in Fig. 7B were comparable to the XPS measured loss in the C–C/CH_2 component in Fig. 5. Conversely, the ATR-FTIR peak intensity at 1083 cm^{-1} increased with UV exposure. The maximum at 1083 cm^{-1} initially declined by approximately 25% after 4 d before steadily rising over 24 d of UV exposure to nearly approximately 180% of its initial value. Additionally, the spectral profile (1000 to 1200) cm^{-1} transformed during exposure from three separate peaks into a single, broad peak with a single, new local maximum at 1070 cm^{-1}. This change in profile and peak maximum is consistent with previously reported IR spectra of silica, including the smaller frequency increases at 800 cm^{-1} and the shoulder near 1200 cm^{-1}.[32,33] Therefore, the C–O stretching frequencies of

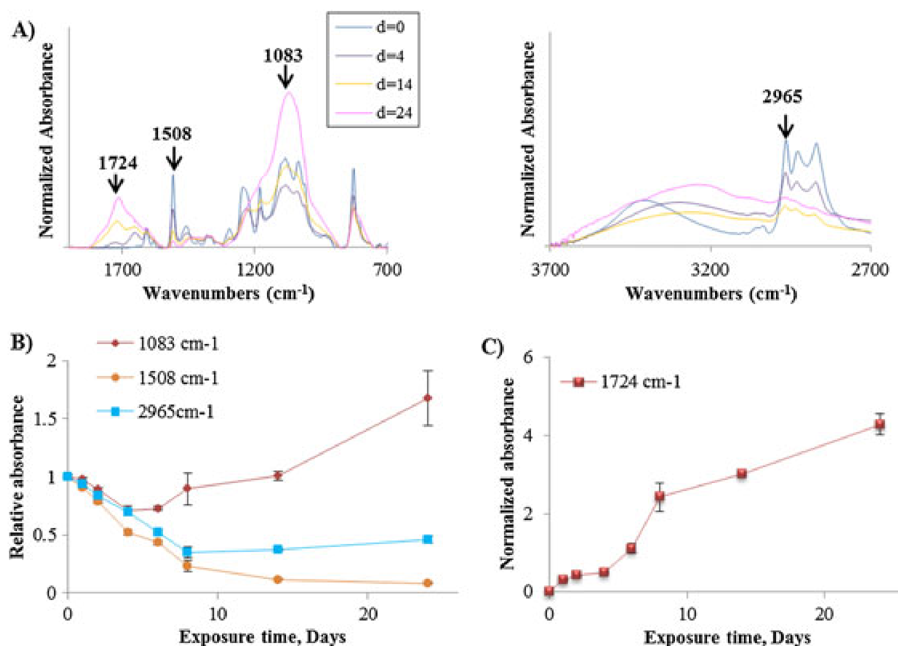

Figure 7. ATR-FTIR results are presented for UV-irradiated SiNCs. A) (left) spectra in the 700 cm^{-1} to 1900 cm^{-1} region with IR absorption intensities from Si–O, aromatic and carbonyl bands; (right) expanded spectra in the 2700 cm^{-1} to 3700 cm^{-1} region, showing contributions from C–H stretching and –OH/NH stretching bands. B) Plots of select peaks from the ATR-FTIR spectra representative of loss in aliphatic (2965 cm^{-1}) and aromatic carbon (1508 cm^{-1}) functionality *versus* UV exposure and increases at 1083 cm^{-1} representing contributions from the SiNPs. C) Plots of select IR relative peak intensity representative of product formation *versus* UV exposure. 1724 cm^{-1} is assigned to the formation of carbonyl functionality. All plotted ATR-FTIR intensity results were the average and standard deviation of four specimens.

Published 2012. This article is a U.S. Government work and is in the public domain in the USA.

the epoxy structure could explain the initial loss of intensity. The rapid increase in intensity is attributed to an increase in the surface concentration of SiNP, consistent with the XPS measured increase in the Si (2p) region after eight days of UV exposure (Fig. 4).

The increase centered at 1724 cm^{-1} is linked to the increase in oxidation of the remaining carbon from the epoxy. Indeed, the spectral feature represented by the measured intensity at 1724 cm^{-1} (Fig. 7A, Left) and plotted *versus* UV exposure (Fig. 7C), possesses a minimum of three components with shoulders at higher and lower wavenumbers (approximately 1650 cm^{-1} and 1770 cm^{-1}). At short exposures, the observed relative IR intensity at 1650 cm^{-1} and 1724 cm^{-1} increased, with the intensity of the former band being the dominant species present in the sample. As the exposures increased past 8 d, however, the intensity at 1724 cm^{-1} became the dominant peak present in the region, and there was the addition of a shoulder at approximately 1770 cm^{-1}. The increase in IR absorption intensity in this region typically signals the formation of carbonyls and other bonds within the sample including: (i) amides and/or alkenes (approximately 1650 cm^{-1}); (ii) carboxylic acids and /or ketones (approximately 1714 cm^{-1}); (iii) esters, various carbonates and/ or acid halides (approximately 1750 cm^{-1}) and (iv) lactones (approximately 1770 cm^{-1}).[31] While it is difficult to separate out which type of functionality is associated to a give spectral feature, it can be asserted that these features are likely to all contribute to increase the overall state of oxidation within the epoxy component of the SiNCs. The 1724 cm^{-1} peak *versus* UV exposure time (Fig. 7C) increased in a manner consistent with the CN(O) / CO(O) XPS component (Fig. 5) suggesting that the carbon associated with the 1724 cm^{-1} stretching frequency has a local chemical environment comparable to a carboxylic acid, ester and/or amide.

Discussion

The photodegradation of SiNCs can be summarized up pictorially in Fig. 8. At short UV exposures ($t_{exp} < 14$ d, Fig. 8 Center), SiNCs exhibited physical transformations characterized by an irregular and rough morphology from its initial smooth characteristics (Fig. 8, Left). This was confirmed with AFM (Fig. 2) where after 4 d of exposure, the RMS roughness increased from 13.09 nm to 30.47 nm in part due to the formation of pitting. Because EDS and XPS analysis demonstrated some loss in carbon concentration at these early exposures, the morphological changes can be attributed to the formation and subsequent removal of oxidized carbon as observed from the XPS analysis (Figs. 3 and 4). The most obvious evidence for early surface oxidation of carbon is the highly oxidized component, CO(O) / CN(O), within the C (1s) region that grew in rapidly over the first eight days (Fig. 5). Correspondingly, the O (1s) signal also increased to nearly 30% of the surface composition from just over 17% (Fig. 4). As a result of only minor increases in the Si (2p) counts at short UV exposures, it is reasonable to attribute most of the increased oxygen content, roughness and pitting to the removal of the epoxy. ATR-FTIR results were consistent with the XPS data and indicated an early rise within the carbonyl stretching frequencies (Fig. 7) after short UV exposures. Furthermore, due to the increased bulk sensitivity associated with ATR (for the incident angle and prism used in this study, the sampling depth is in the 500 nm to 2500 nm range) compared to XPS (approximately 10 nm), these FTIR results also suggest that the oxidation of carbon is occurring further into the material.

The surface chemical and morphological characteristics continued to transform with increasing UV exposure (Fig. 8, right). Morphologically, the surface of the SiNCs became increasingly rough with raised, plate-like features after long UV exposures (Fig. 1 A, Fig. 2 C and SI Fig. S2). Consistent with observations from the images, the AFM measured RMS roughness increased to a value of 129.29 nm. Furthermore, evidence for cracking was also apparent (SI Fig. S1), which is consistent with previous reports of declining materials properties when the mass fraction of SiNPs is excessively high.[1] The distribution of carbon functionalities at the surface and into the bulk continued to change with increasing UV exposure as the carbon concentration decreased to less than 50% of initial concentration (Figs.s 1B, 3 and 4) due to a loss in the initial epoxy components (Fig. 3 and 5). Once again, the ATR-FTIR analyses support this, reflecting a nearly complete loss in most of the initial absorption bands present in the initial, unexposed SiNCs, providing additional confirmation that this process occurred well into the bulk of the material.

As opposed to short exposures of UV radiation, the long exposures clearly increased the SiNP surface concentration as a result of the epoxy's oxidative removal as displayed in Fig. 8. XPS elemental analysis (Figs. 3 and 4) revealed a significant increase in surface silicon concentration to a final percent surface concentration of (21.23 ± 1.88) % at 35 and greater days of exposure, which translates to an increase from a 10% mass fraction to approximately 73.5% mass fraction of SiNPs. EDS (Fig. 1B) and ATR-FTIR analysis (Fig. 7 C), both possessing a greater sampling depth (500 nm to 2500 nm) than XPS, revealed an increased SiNP concentration through increased relative intensities of the Si Kα and the Si–O stretch, respectively. Therefore, while the thickness of the layer for increased (SiNP) cannot be accurately identify, ATR-FTIR and EDS results strongly support the assertion that the UV-induced enhancement in the surface concentration of SiNP continued into the SiNC bulk. Specifically, if the increase of SiNP mass fraction, or the aforementioned transformations of the epoxy, were only within the top 10 nm of the SiNC, the enhancement of silicon-related signal would only be

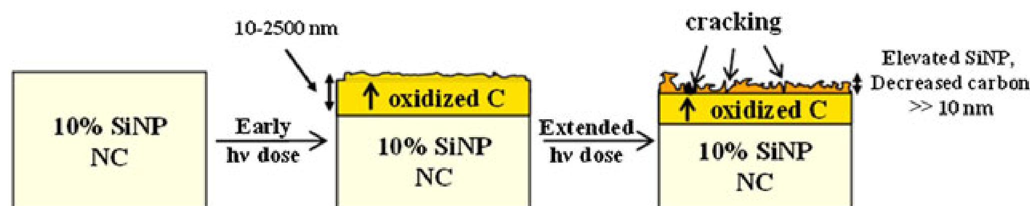

Figure 8. Route of UV degradation of 10% (by mass) SiNP–epoxy composite. After initial UV exposure, the surface of the SiNC roughens, and the top portion of the composite increases in oxidized carbon content and correspondingly decreases from the initial aromatic, aliphatic and C–O functional groups. At extended exposures, the carbon from the epoxy continues to oxidize and is eventually removed. The SiNP concentration increases at the surface and into the bulk. The chemical transformations at surface resulted in a further increases in surface pitting and cracking.

Published 2012. This article is a U.S. Government work and is in the public domain in the USA.

generated from less than 2% of the sampling volume for ATR-FTIR and EDS, effectively yielding a much smaller increase in signal.

From the early losses of the initial carbon components, including the aromatic carbon, aliphatic carbon and the C–O stretch, along with the steady increase of the nitrogen and carbonyl concentrations, it is reasonable to assume that one early point (prior to 14 days) of photo-induced oxidation occurred within the DGEBA branches of the epoxy. Longer exposures, which continued to remove a majority of the epoxy components from the SiNC surface which, as a consequence, resulted in an increased surface concentration of SiNPs as indicated by increased silicon and oxygen concentrations. From the loss of the aromatic features and nitrogen increases, two potential processes can be hypothesized: (i) modifications in the aromatic structure associated with DGEBA's phenyl groups transforming via photo-oxidation into volatile and/or non-volatile byproducts, or (ii) oxidative removal of phenyl ring segments of DGEBA through the formation of large volatile organic fragments (chain scission) or by physical mechanisms. However, previous work on UV-exposed SiNC demonstrated a significant mass loss prior to any large increases in the SiNP surface concentration,[17,18] while others have reported various volatile species forming along with chain scissions events by photodegradation of comparable epoxy samples.[11,13,15,34,35] This suggests that the early UV-induced loss of the initial carbon components in this study was a result of removing carbon-based components and not due to transformed carbon components left behind as non-volatile, non-aromatic compounds. While fully mapping out the reaction sequence is beyond the scope of the current study, it can be stated that photo-oxidative removal of the epoxy, via chain scission and/or volatilization of smaller organic fragments, would result in a roughened SiNC surface, an enhanced SiNP concentration and highly oxidized residual carbon.

Conclusions

The analysis of the photo-induced, surface transformations of SiNCs exposed to 290-nm to 400-nm UV radiation has been presented. Surface analytical techniques have confirmed that photodegradation of the SiNC surface proceeded through an oxidative removal of a large portion of the epoxy. The degradation and removal of the matrix layer near the surface resulted in an increased mass fraction of SiNPs at the composite surface with UV exposure. Techniques with increased bulk sensitivity (ATR-FTIR, EDS) demonstrated that the SiNC photodegradation continued into the bulk of the material (> 10 nm). This study demonstrates the utility of combining orthogonal surface chemical analyses in determining the level of UV-induced degradation in a SiNC. From an environmental, health and safety perspective, we have demonstrated that these SiNCs remain at low silicon surface concentrations up through eight days of UV exposure (290 nm to 400 nm) at 22 times the power of the sun. Since, significant SiNP release from the composite surface is not likely to occur prior to a large increase in the silicon surface concentration within the top 10 nm, this provides an efficient method for determining the effective lifetime of comparable SiNCs when in service.

Acknowledgement

JMG would like to acknowledge the National Research Council for funding his postdoctoral fellowship.

References

[1] H. Zou, S. S. Wu, J. Shen, Polymer/silica nanocomposites: Preparation, characterization, properties, and applications. *Chem. Rev.* **2008**, *108*(9), 3893–3957.
[2] C. A. Wilkie, A. B. Morgan, *Fire retardancy of polymeric materials*, (2nd edn), CRC Press, Boca Raton, **2010**.
[3] BYK Additives and Instruments www.byk.com/en/additives/nanobyk/scratch-resistance.html **2011**.
[4] Nissan Chemical company www.nissanchem-usa.com **2011**.
[5] A. C. Balazs, T. Emrick, T. P. Russell, Nanoparticle polymer composites: Where two small worlds meet *Science*, **2006**, *314*(5802), 1107–1110.
[6] R. Lach, *et al.*, Indentation Fracture Mechanics for Toughness Assessment of PMMA/SiO2 Nanocomposites. *Macromol. Mater. Eng.* **2006**, *291*(3), 263–271.
[7] X.-Y. Shang, *et al.*, Compatibility of Soluble Polyimide/Silica Hybrids Induced by a Coupling Agent. *Chem. Mater.* **2002**, *14*(1), 71–77.
[8] M. Garcia, *et al.*, Friction and wear studies on nylon-6/SiO2 nanocomposites, *J. Appl. Polym. Sci.* **2004**, *92*(3), 1855–1862.
[9] N. Lucas, *et al.*, Polymer biodegradation: Mechanisms and estimation techniques – A review, *Chemosphere* **2008**, *73*(4), 429–442.
[10] J. Gorham, *et al.*, Surface reactions of molecular and atomic oxygen with carbon phosphide films. *J. Phys. Chem. B*, **2005**. *109*(43), 20379–20386.
[11] J. F. Rabek, *Polymer Photodegradation: Mechanisms and Experimental Methods* **1995**, *New York*, NY: Chapman Hall.
[12] B. Singh, N. Sharma, Mechanistic implications of plastic degradation. *Polym. Degrad. Stab.*, **2008**. *93*(3), 561–584.
[13] N. Grassie, M. I. Guy, N. H. Tennent, Degradation of Epoxy Polymers .5. Photodegradation of Bisphenol-a Diglycidyl Ether Cured with Ethylene Diamine, *Polym. Degrad. Stab.* **1986**, *14*(3), 209–216.
[14] N. Mailhot, *et al.*, Study of the degradation of an epoxy/amine resin, 1 photo- and thermo-chemical mechanisms, *Macromol. Chem. Physic.* **2005**, *206*(5), 575–584.
[15] A. Rivaton, L. Moreau, J. L. Gardette, Photo-oxidation of phenoxy resins at long and short wavelengths - I. Identification of the photo-products, *Polym. Degrad. Stab.* **1997**, *58*(3), 321–332.
[16] A. Rivaton, L. Moreau, J. L. Gardette, Photo-oxidation of phenoxy resins at long and short wavelengths - II. Mechanisms of formation of photoproducts, *Polym. Degrad. Stab.* **1997** *58*(3), 333–339.
[17] T. Nguyen, *et al.*, Fate of nanoparticles during life cycle of polymer nanocomposites, *J. Phys. Conf. Ser.* **2011**, *304*, 012060.
[18] T. Nguyen, *et al.*, Characterization of Surface Accumulation and Release of Nanosilica During Irradiation of Polymer Nanocomposites with Ultraviolet Light, *J. Nanosci. Nanotech.* **2012**, in press.
[19] J. Chin, *et al.*, Accelerated UV weathering device based on integrating sphere technology. *Rev. Sci. Instrum.*, **2004**, *75*(11), 4951–4959.
[20] N. Ritchie, DTSA II, National Institute of Standards and Technology: Gaithersburg, MD. p. Retrieved from Public Domain Software Available from NIST: http://www.cstl.nist.gov/div837/837.02/epq/dtsa2/index.html, **2008**.
[21] J. F. Molder, *et al.*, In *Handbook of X-ray Photoelectron Spectroscopy*, ed. J. Chastain, Eden Prairie, Perkin-Elmer Corporation, **1992**.
[22] J. Gorham, B. Smith, D. H. Fairbrother, In Modification of alkanethiolate self-assembled monolayers by atomic hydrogen: Influence of alkyl chain length, *J. Phys. Chem. C* **2007**, *111*(1), 374–382.
[23] T. Sugama, *et al.*, Study of Interactions at Water-Soluble Polymer Ca(OH)2 or Gibbsite Interfaces by Xps, *Cement Concrete Res.* **1989**, *19*(6), 857–867.
[24] M. Gervais, *et al.*, Surface Studies of Polypeptidic Block Copolymers by Electron-Spectroscopy for Chemical-Analysis - Poly(N-Epsilon-Trifluoroacetyl-L-Lysine)-Polysarcosine Diblock Copolymers, *Polymer*, **1986**, *27*(10), 1513–1520.
[25] L. J. Gerenser, Photoemission Investigation of Silver Poly(Ethylene-Terephthalate) Interfacial Chemistry - the Effect of Oxygen-Plasma Treatment, *J. Vac. Sci. Technol. A.* **1990**, *8*(5), 3682–3691.
[26] M. Morra, *et al.* On the Aging of Oxygen Plasma-Treated Polydimethylsiloxane Surfaces, *J. Colloid Interf. Sci.* **1990**, *137*(1), 11–24.
[27] J. A. Gardella, *et al.* Pi-Star[−Pi Shakeup Phenomena in Organic Polymers with Backbone Aromatic Functionality, *J. Electron Spectrosc.* **1984**, *34*(1), 97–102.

Published 2012. This article is a U.S. Government work and is in the public domain in the USA.

[28] J. Mathias, G. Wannemacher, Basic Characteristics and Applications of Aerosil .30. The Chemistry and Physics of the Aerosil Surface, *J. Colloid Interf. Sci.*, **1988**, *125*(1), 61–68.
[29] A. Kumar, *et al*. Fabrication of Minority-Carrier-Limited Normal-Si/Insulator Metal Diodes, *Appl. Phys. Lett.* **1990**, *56*(19), 1919–1921.
[30] A. Cros, *et al*. An X-Ray Photoemission Spectroscopy Investigation of Oxides Grown on Auxsi1-X Layers, *J. Appl. Phys.* **1990**, *67*(4), 1826–1830.
[31] R. A. Meyers, In *Encyclopedia of analytical chemistry: applications, theory, and instrumentation*, Wiley, Chichester; New York, **2000**.
[32] A. Bertoluzza, *et al*. Raman and Infrared-Spectra on Silica-Gel Evolving toward Glass, *J. Non-Cryst. Solids* **1982**, *48*(1), 117–128.
[33] J. R. Martınez, *et al*. Infrared spectroscopy analysis of the local atomic structure in silica prepared by sol–gel, *J. Chem. Phys.* **1998**, *109*(17), 7511.
[34] N. Grassie, M. I. Guy, N. H. Tennent, Degradation of epoxy polymers: 3—Photo-degradation of bisphenol-A diglycidyl ether, *Polym. Degrad. Stab.* **1985**, *13*(3), 249–259.
[35] L. Monney, *et al*. Trapping and identification of volatile photo-products of a photo-oxidised epoxy matrix, *Polym. Degrad. Stab.* **1999**, *66*(1), 17–22.

Published 2012. This article is a U.S. Government work and is in the public domain in the USA.